J. Phys. A: Math. Theor. **43** (2010) 415302 (15pp) doi:10.1088/1751-8113/43/41/415302

Quantum backflow, negative kinetic energy, and optical retro-propagation

M V Berry

H H Wills Physics Laboratory, Tyndall Avenue, Bristol BS8 1TL, UK

Received 6 August 2010
Published 27 September 2010
Online at stacks.iop.org/JPhysA/43/415302

Abstract
For wavefunctions whose fourier spectrum (wavenumber or frequency) is positive, the local phase gradient can sometimes be negative; examples of this 'backflow' occur in quantum mechanics and optics. The backflow probability P (fraction of the region that is backflowing) is calculated for several cases. For waves that are superpositions of many uncorrelated components, $P = (1 - r)/2$, where r is a measure of the dispersion (mean/r.m.s.) of the component frequencies or wavenumbers. In two dimensions (backflow in spacetime, or wave propagation in the plane) the boundary of the backflowing region includes the phase singularities of the wave.

PACS numbers: 02.30.Nw, 02.50.Ey, 02.65.Vf, 03.65.Ta, 42.25.Fx, 42.30.Kq

1. Introduction

It might seem that a complex wavefunction containing only wavenumbers that are positive semidefinite, namely

$$\psi(x) = \sum_{n=0}^{N} c_n \exp(\mathrm{i}k_n x), \qquad k_n \geqslant 0, \qquad c_n \text{ complex} \tag{1.1}$$

must always represent a wave travelling forwards, that is, towards positive x. But this need not be true. To understand why, consider the same function written not as an $N + 1$ wave superposition but in the amplitude-phase form

$$\psi(x) = \rho(x) \exp\left\{\mathrm{i}\int_0^x \mathrm{d}x' k(x')\right\}, \tag{1.2}$$

in which both the amplitude $\rho(x)$ and the local wavenumber

$$k(x) = \partial_x \arg\psi(x) = \partial_x \operatorname{Im}\log\psi(x) = \operatorname{Im}\frac{\partial_x\psi(x)}{\psi(x)} \tag{1.3}$$

are real. When $k(x) > 0$, the wave is locally travelling forwards, and when $k(x) < 0$ it is travelling backwards. It is known ([1], especially Appendix C, and [2]) that $k(x) < 0$ can

occur for waves of the form (1.1), that is, waves containing only positive momenta can travel backwards in certain regions of the x axis.

This phenomenon is known as 'backflow', and my aim here is to understand some aspects of it and related effects. A previous study [2] has explored the probability that a quantum free particle, in a state consisting only of positive momenta, will be detected on the half-line $x < 0$; backflow can, counterintuitively, cause this quantity to increase as the state evolves. And unexpected connections were discovered [1, 3] between backflow and quantum arrival times, and explored in detail (see [4], especially section 5.3). Here the emphasis will be rather different: I will concentrate on the distribution and evolution of the regions of the x axis for which $k(x) < 0$, that is, the backflowing regions.

Section 2 gives the simple introductory example of a two-wave superposition: $N = 1$ in (1.1). Then, section 3 is a calculation of the probability that a given x lies in a region of backflow, that is, the measure of the backflowing regions, for the case $N \gg 1$ in (1.1), where the superposition contains many fourier components which are uncorrelated. The result extends recent studies [5, 6] of the statistics of wavevectors in random waves. It is possible to construct many-wave superpositions in which the components are strongly correlated, and for which the backflow probability approaches the maximum value of $1/2$; this 'strong backflow'is illustrated in section 5.

If $\psi(x)$ in (1.1) represents the initial state of a quantum wavefunction $\Psi(x, t)$ evolving freely according to the Schrödinger equation, it is natural to ask how the backflowing regions evolve, that is, what are the shapes of the regions $k(x, t) < 0$ in spacetime. This question is addressed in section 5. Associated with the time-development of the wave is the local frequency

$$\omega(x, t) = -\mathrm{Im}\,\partial_t \log \Psi(x, t) = -\mathrm{Im}\frac{\partial_t \Psi(x, t)}{\Psi(x, t)}. \tag{1.4}$$

For superpositions in which all component frequencies are positive, the wave in optical terminology is the 'analytic signal' [7], and $\omega(x, t) < 0$ corresponds to events for which the local frequency is negative. If the waves represent quantum particles, $\omega(x, t) < 0$ corresponds to negative energy. This is also discussed in section 5. For particles governed by the Dirac equation, it raises the intriguing possibility that particles might sometimes (literally: for some time intervals) masquerade as antiparticles.

Section 6 concerns an alternative interpretation of backflow, in which (1.1) represents the $z = 0$ section of a monochromatic optical wave $\Psi(x, z)$ propagating into the half-plane $-\infty < x < +\infty, \quad 0 \leqslant z < \infty$, and governed by the Helmholtz equation with wavenumber k_0. Then backflow corresponds to places in the plane where the wave is locally travelling to the left even though all component waves are right-moving. For a wave propagating towards positive z, all z components of the constituent wavevectors are positive. Nevertheless, the z component of the local wavevector, namely

$$k_z(x, z) = -\mathrm{Im}\,\partial_z \log \Psi(x, z) = -\mathrm{Im}\frac{\partial_z \Psi(x, z)}{\Psi(x, z)}, \tag{1.5}$$

can be negative, and regions of the plane corresponding to 'retro-propagation' are also studied in section 6.

For these cases involving two variables (e.g. x, t or x, z), the points of phase singularity (optical vortices), where $\Psi = 0$, must lie on the boundaries of the backflowing or retro-propagating regions. Moreover the boundary curve at such points must be tangent to the direction of the relevant component of the phase gradient. To show this, consider retro-propagation, and a wave with a zero at $x = 0$, $z = 0$. The local form is

$$\Psi(x, z) = ax + bz + \cdots (a, b \text{ complex}), \tag{1.6}$$

so (1.5) gives

$$k_z(x,z) = \mathrm{Im}\,\frac{b}{ax+bz} = \frac{x}{|ax+bz|^2}\,\mathrm{Im}\,a^*b. \tag{1.7}$$

Thus, locally, the retro-propagation boundary is $x = 0$, that is, tangent to the z direction.

Returning to (1.3), we remark that $k(x)$ can be regarded, apart from a factor $\hbar$, as the local expectation value of the momentum operator. This can easily be seen using operator and Dirac notation: a short calculation gives

$$k(x) = \partial_x\,\mathrm{Im}\log\langle x/\psi\rangle = \frac{\langle\psi|\frac{1}{2}(\delta(x-\hat{x})\hat{k}+\hat{k}\delta(x-\hat{x}))|\psi\rangle}{\langle\psi|\delta(x-\hat{x})|\psi\rangle} \tag{1.8}$$

where, in position representation,

$$\langle x|\hat{k}|\psi\rangle = -\mathrm{i}\partial_x\psi(x) \tag{1.9}$$

Backflow is closely related to superoscillation [8–10], in which waves vary on scales unrepresented in their fourier spectrum. More generally the local wavenumber can be regarded as the result of a 'weak measurement' [11] A_{weak} of the operator $\hat{A} = \hat{k}$ in the preselected state $|\psi\rangle$, with the state $|\phi\rangle = |x\rangle$ postselected. The reason is that, as a short calculation shows, general theory gives, for this case of a weak measurement of momentum with position postselected,

$$A_{\mathrm{weak}} = \mathrm{Re}\,\frac{\langle\phi|\hat{A}|\psi\rangle}{\langle\phi/\psi\rangle} = k(x), \tag{1.10}$$

with $k(x)$ given by (1.3) or (1.4).

2. Two interfering waves

The simplest wave illustrating backflow (echoing an earlier study [2]) is

$$\psi(x) = 1 - a\exp(\mathrm{i}x), \tag{2.1}$$

for which (1.3) gives the local wavenumber

$$k(x) = a\frac{(a-\cos x)}{1+a^2-2a\cos x}. \tag{2.2}$$

In this periodic function, backflow occurs for $a < 1$, within the interval $|x| < \arccos a$ (see figure 1). As a gets smaller, the backflowing region gets wider, and as a approaches zero it grows to occupy half the x axis. The backflowing fraction of the x axis is (cf (3.1) to follow)

$$P_{\mathrm{back}} = \frac{\cos^{-1}a}{\pi}. \tag{2.3}$$

3. Backflow statistics for typical many-wave superpositions

The backflow probability P_{back} is the fraction of the x axis for which $k(x) < 0$, that is

$$P_{\mathrm{back}} = \lim_{L\to\infty}\frac{1}{2L}\int_{-L}^{L}\mathrm{d}x\,\Theta(-k(x)) = \int_{-\infty}^{0}\mathrm{d}k\,P_k(k), \tag{3.1}$$

in which Θ is the unit step function and P_k is the probability density of the local wavenumber, namely

$$P_k(k) = \lim_{L\to\infty}\frac{1}{2L}\int_{-L}^{L}\mathrm{d}x\,\delta(k-k(x)). \tag{3.2}$$

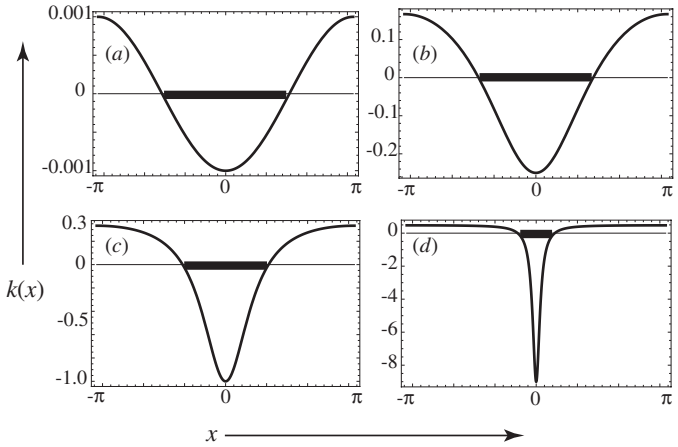

Figure 1. Local wavenumber $k(x)$ (equation (2.2)) for the two-wave superposition (2.1), with the regions of backflow indicated by black bars, for (*a*) $a = 0.001$, (*b*) $a = 0.2$, (*c*) $a = 0.5$, (*d*) $a = 0.9$. Note the decreasing width of the region of backflow as a increases and the degree of backflow increases, i.e. as $k(x)$ reaches larger negative values.

For $N \gg 1$ and uncorrelated amplitudes c_n in (1.1), the central limit theorem implies that real and imaginary parts $u(x)$ and $v(x)$ can be regarded as gaussian random functions, enabling the integrals over x to be replaced by ensemble averages, using (cf (1.3))

$$k(x) = \frac{u(x)\partial_x v(x) - v(x)\partial_x u(x)}{u(x)^2 + v(x)^2}. \tag{3.3}$$

A complication for functions of the type (1.1), where the spectrum of component wavenumbers is unsymmetrical (all $k_n \geqslant 0$), is that although u and v are independent identially distributed random variables, as are $\partial_x u$ and $\partial_x v$, u and $\partial_x v$ are correlated, as are v and $\partial_x u$. The direct calculation can still be performed, but it is easier to bypass it by using the following adaptation of a known result.

For an operator $\hat{A}$ with many eigenvalues A_n symmetrically distributed in the range $-A_{\max} \leqslant A_n \leqslant +A_n$, the probability distribution of weak values A_{weak}, with randomly chosen pre- and post-selected states, takes the recently-derived universal form [12]

$$P(A_{\text{weak}}) = \frac{\langle A_n^2 \rangle}{2\left(A_{\text{weak}}^2 + \langle A_n^2 \rangle\right)^{3/2}}, \tag{3.4}$$

where here and hereafter $\langle \cdots \rangle$ denotes an ensemble average (not quantum expectation values as in section 1). Specialising to a distribution of positive semidefinite wavenumbers as in (1.1), by writing

$$A_{\text{weak}} = -A_{\max} + k, \qquad A_n = -A_{\max} + k_n, \tag{3.5}$$

(3.4) becomes

$$P_k(k) = \frac{\langle k_n^2 \rangle - \langle k_n \rangle^2}{2\left(k^2 - 2k\langle k_n \rangle + \langle k_n^2 \rangle\right)^{3/2}}. \tag{3.6}$$

Here

$$\langle k_n \rangle = \frac{\sum_{k=0}^{N} |c_n|^2 k_n}{\sum_{k=0}^{N} |c_n|^2}, \qquad \langle k_n^2 \rangle = \frac{\sum_{k=0}^{N} |c_n|^2 k_n^2}{\sum_{k=0}^{N} |c_n|^2}. \tag{3.7}$$

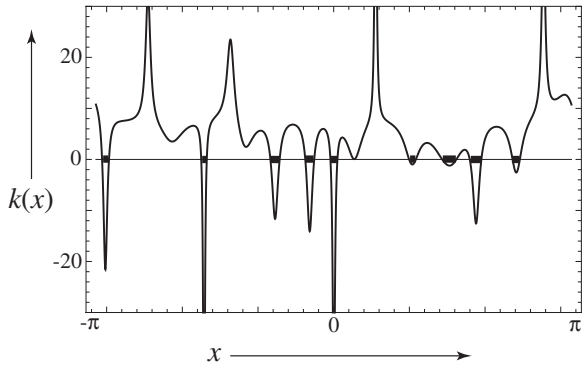

Figure 2. Local wavenumber $k(x)$ (equation (2.2)) for the 20-wave superposition (3.10), with the regions of backflow indicated by black bars.

For the backflow probability, (3.1) now gives, as the main result of this section,

$$P_{\text{back}} = \frac{1 - r_{\text{back}}}{2}, \tag{3.8}$$

where

$$r_{\text{back}} \equiv \frac{\langle k_n \rangle}{\sqrt{\langle k_n^2 \rangle}}. \tag{3.9}$$

Thus the backflow probability depends on how the component momenta k_n are distributed: P_{back} is larger if the spread is larger, and approaches its maximum value $1/2$ when $\langle k_n^2 \rangle \gg \langle k_n \rangle^2$. Figure 2 shows a sample graph of $k(x)$, for which, in (1.1)

$$\begin{aligned} &N = 20, \qquad k_n = n, \qquad c_0 = 0, \qquad c_{n>0} = \frac{1}{\sqrt{n}} \exp(\mathrm{i}\phi_n) \\ &\phi_n = \text{random on } [0, 2\pi] \end{aligned} \tag{3.10}$$

(this superposition is periodic in x with period 2π). From (3.8) and (3.9), the predicted value of P_{back} is 0.136, and the measured backflow fraction is $P_{\text{back}} = 0.163$, which for such a small sample (nine backflow regions per period) constitutes reasonable agreement.

4. Strong backflow

The function

$$\psi(x) = (1 - a\exp(\mathrm{i}x))^N, \qquad N \gg 1, \qquad a < 1 \tag{4.1}$$

is a simple generalization of (2.1), and a variant of a function studied previously [10] in the context of superoscillations. It has the form (1.1), with

$$k_n = n, \qquad c_n = (-a)^n \frac{N!}{n!(N-n)!}. \tag{4.2}$$

Although none of the k_n are negative, the local wavenumber (cf (2.2))

$$k(x) = Na\frac{(a - \cos x)}{1 + a^2 - 2a\cos x} \tag{4.3}$$

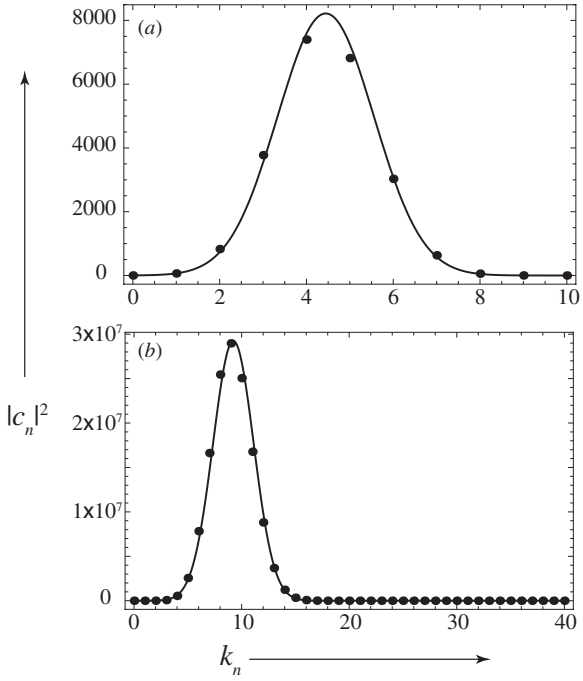

Figure 3. Power spectrum $|c_n|^2$ of the wave (4.1), for (*a*) $N = 10$, $a = 0.8$; (*b*) $N = 40$, $a = 0.3$. Dots: exact spectrum (4.2); curves: approximation (4.5).

is negative near $x = 0$ for $a < 1$, the largest backflow being

$$k(0) = -\frac{Na}{1-a} \tag{4.4}$$

The dramatic nature of this backflow can be seen from the power spectrum $|c_n|^2$ of $\psi(x)$, which is closely approximated (figure 3) by a gaussian for $N \gg 1$: Stirling's formula gives

$$|c_n|^2 \approx \frac{(1+a)^{2N+2}}{2\pi Na} \exp\left\{-\frac{(1+a)^2}{Na}\left(n - \frac{Na}{1+a}\right)^2\right\}. \tag{4.5}$$

This is strongly peaked about the mean value

$$\langle k_n \rangle \approx \frac{Na}{1+a}, \tag{4.6}$$

which of course lies between 0 and N, in contrast to $k(0)$, which from (4.4) lies completely outside the spectrum.

The wave (4.1) has the same backflow fraction P_{back} of the x axis as (2.1), namely (2.3). This is much larger than the value (3.8) that would be predicted on the basis of the power spectrum (4.5) if the phases in the superposition were random, which would be

$$P_{\text{back}} \approx \frac{1}{8Na} \tag{4.7}$$

– small for $N \gg 1$, because the k_n spectrum is concentrated near $\langle k_n \rangle$. Of course, the large value of P_{back} arises because the phases in (4.1) are not random.

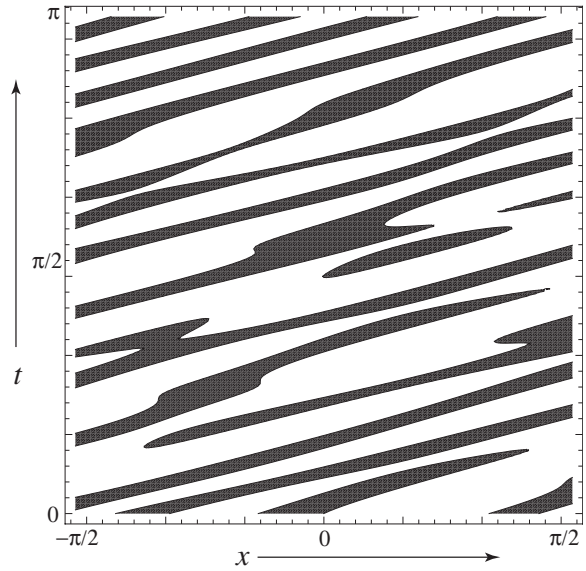

Figure 4. Backflow regions in spacetime (black) in the random wave (5.2) and (5.4).

5. Quantum backflow and negative energy in spacetime

Now consider the state $\psi(x)$ in (1.1) as the initial form $\Psi(x, 0)$ of a quantum state $\Psi(x, t)$ evolving according to the Schrödinger equation

$$\mathrm{i}\partial_t \Psi\,(x,t) = -\tfrac{1}{2}\partial_x^2 \Psi(x,t), \tag{5.1}$$

that is

$$\Psi\,(x,t) = \sum_{n=0}^{N} c_n \exp\left\{\mathrm{i}\left(k_n x - \tfrac{1}{2}k_n^2 t\right)\right\}, \tag{5.2}$$

or the alternative form

$$\Psi(x,t) = \frac{1}{\sqrt{2\pi \mathrm{i} t}} \int_{-\infty}^{\infty} \mathrm{d}x' \psi(x') \exp\left\{\mathrm{i}\frac{(x'-x)^2}{2t}\right\}. \tag{5.3}$$

It is natural to study the shape of the region $k(x, t) < 0$ in spacetime, to understand how the regions of backflow evolve. For the random superpositions considered in section 3, we expect the the measure P_{back} of the backflowing regions to be conserved on the average, because the result (3.7) depends only on the power spectrum of the superposition, which is unchanged by propagation, and on the assumption of random phases, which is unaffected by the additional phases $-k_n^2 t/2$ in (5.2). The approximate conservation of P_{back} is illustrated in figure 4 for the 9-wave superposition

$$\begin{aligned} &N = 8, \qquad k_n = n, \qquad c_0 = 5, \qquad c_{n>0} = \exp(\mathrm{i}\phi_n) \\ &\phi_n = \text{random on } [0, 2\pi\,] \end{aligned} \tag{5.4}$$

(as well as being periodic in x with period 2π, this superposition is periodic in t with period 4π, that is, it exhibits quantum revivals). The velocity of the backflowing regions, that is, the

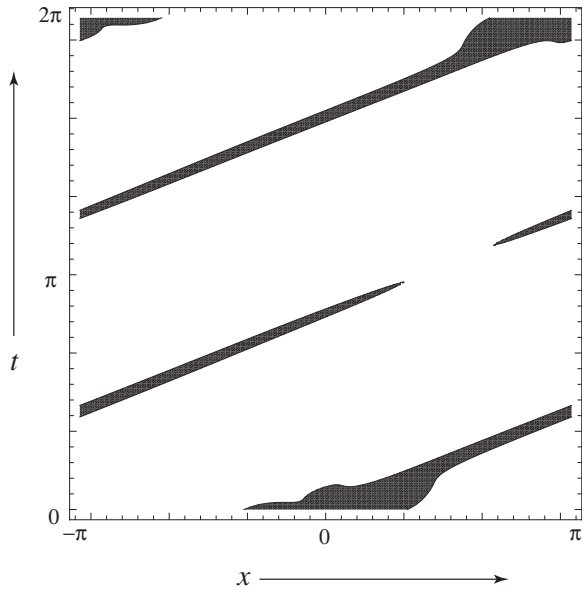

Figure 5. As figure 4, for the evolution of the strongly backflowing initial wave (4.1) with $a = 0.5$ and $N = 6$.

slope of the black stripes in figure 4, is explained in terms of the largest fourier component in (5.2): the slope should be $x/t \sim k_N/2$, which for (5.2) is 4, approximately as observed.

The situation is different for non-random initial superpositions such as (4.1) in which the P_{back} is large. There, evolution soon destroys the delicate conspiracy of phases responsible for the strong backflow, and reduces P_{back} to values comparable with those expected from random superpositions (equation (3.8)). Figure 5 shows the strong backflow rapidly shrinking, as well as the quantum revival at $t = 2\pi$ which is a consequence of the initial $\psi(x)$ being periodic.

As N increases, the destruction of strong backflow exhibits a certain universality. The form (1.2), together with the fact that $k(x)$ is proportional to N (equation (4.3)), suggests changing variables to

$$k(x) = N\kappa(x), \qquad t = \frac{\tau}{N}, \tag{5.5}$$

so the phase in the integral (5.3) becomes

$$N\left(\int_0^{x'} \mathrm{d}x''\kappa(x'') + \frac{(x-x')^2}{2\tau}\right), \tag{5.6}$$

and applying the method of stationary phase. And indeed, as figure 6 shows, the destruction of backflow takes a similar form for increasing N under N-magnification of the t scale.

But there are subtleties: although the right-hand boundaries of the backflowing regions in figure 6 can be reproduced by the method of stationary phase (I do not give the argument here), the left-hand boundaries exhibit undulations that get finer as N increases. As will be demonstrated now, these are associated wiith the zeros of $\Psi(x, t)$, that is the wavefunction's spacetime vortices, which as was shown in section 1 must lie on the boundary of the region of backflow.

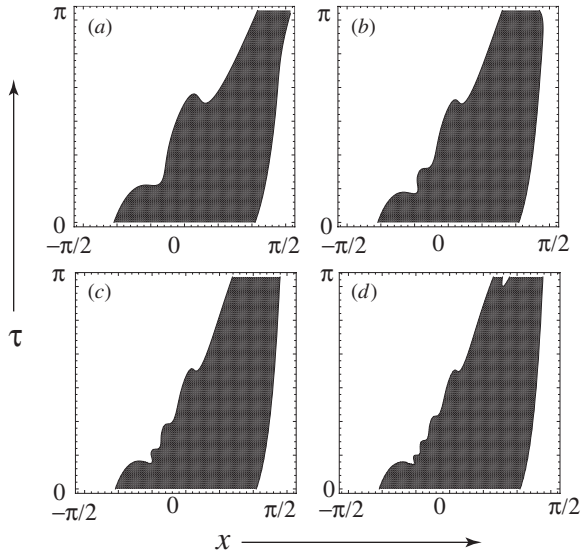

Figure 6. Destruction of strong backflow in the inital stages of evolution, for the initial wave (4.1) with $a = 0.5$ and (*a*) $N = 6$, (*b*) $N = 10$, (*c*) $N = 14$, (*d*) $N = 18$.

For the small t we are interested in, backflow occurs for rather small x, suggesting a linearization of the initial wave (4.1). From the family of possible linearizations

$$\begin{aligned}\psi(x) &= \exp(\mathrm{i}Nx\beta(a))[\exp(-\mathrm{i}x\beta(a)) - a\exp(\mathrm{i}x(1-\beta(a)))]^N \\ &\approx \exp(\mathrm{i}Nx\beta(a))[1-a-\mathrm{i}x(\beta(a)+a(1-\beta(a)))]^N, \end{aligned} \tag{5.7}$$

we choose $\beta(a)$ such that the approximate wavenumber reproduces the zeros of the exact $k(x)$, that is $x = \pm\cos^{-1}a$ (cf (2.2)). This $\beta(a)$ satisfies

$$\frac{a(1-a)}{\beta(a)(a+\beta(a)(1-a))^2} = (\cos^{-1}a)^2 \tag{5.8}$$

($\beta(a)$ increases from 0 to 1/2 as a increases from 0 to 1). Then the evolution integral (5.3) becomes

$$\begin{aligned}\Psi\left(x, \frac{\tau}{N}\right) \approx \frac{1}{\sqrt{2\pi\mathrm{i}t}}\int_{-\infty}^{\infty}\mathrm{d}x'[1-a-\mathrm{i}x'(\beta(a)+a(1-\beta(a)))]^N \\ \times\exp\left\{\mathrm{i}N\left(x'\beta(a)+\frac{(x'-x)^2}{2\tau}\right)\right\}. \end{aligned} \tag{5.9}$$

This can be evaluated exactly in terms of Hermite polynomials, using (cf formula (18.10.7) of [13]))

$$\frac{1}{\sqrt{\pi}}\int_{-\infty}^{\infty}\mathrm{d}s(s-s_0)^N\exp(-s^2) = \left(\frac{\mathrm{i}}{2}\right)^N H_n(\mathrm{i}s_0). \tag{5.10}$$

Thus, in this linearized approximation, the local wavenumber becomes

$$k(x,\tau) = N\beta(a) - \sqrt{\frac{N}{2\tau}}\mathrm{Im}\left[\exp\left(\frac{1}{4}\mathrm{i}\pi\right)\frac{H_N'(X)}{H_N(X)}\right], \tag{5.11}$$

in which

$$X = \sqrt{\frac{N}{2\tau}}\left[\exp\left(-\frac{1}{4}\mathrm{i}\pi\right)\frac{1-a}{a+\beta(a)(1-a)} - \exp\left(\frac{1}{4}\mathrm{i}\pi\right)(x-\tau\beta(a))\right]. \tag{5.12}$$

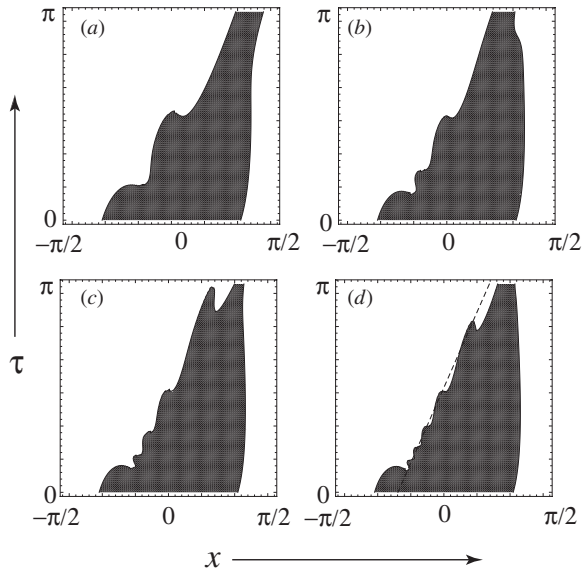

Figure 7. As figure 6, for the approximate wave (5.9) and (local wavenumber (5.11)). The zeros of $\Psi(x, t)$ are located on the line (5.13), shown dashed in (*d*).

As figure 7 illustrates, this reproduces rather accurately the early stages of backflow destruction, including the undulations (cf figure 6). To see the connection with the zeros of $\Psi(x, t)$, we note that the zeros of the Hermite polynomials are real. From (5.12) this implies that the zeros lie on the line

$$x = \tau\beta(a) - \frac{1-a}{a+\beta(a)(1-a)}, \tag{5.13}$$

and figure 7(*d*) shows that this intersects the left-hand boundary of the backflowing region where this is horizontal, as anticipated in section 1.

Consider now the local frequency $\omega(x, t)$, which for waves satisfying (5.1) is the same as the local kinetic energy:

$$\omega(x,t) = -\mathrm{Im}\,\partial_t \log\Psi(x,t) = -\frac{1}{2}\,\mathrm{Re}\,\frac{\partial_x^2\Psi(x,t)}{\Psi(x,t)} \tag{5.14}$$

(this is one of several possible definitions of kinetic energy [14], corresponding to different possible experimental conditions). $\omega(x, t)$ can be negative, even though the component frequencies $\frac{1}{2}k_n^2$ in (5.2) are all positive. The theory of negative energy is similar to that already given for $k(x)$, but some details are different.

For random superpositions, the probability that a spacetime event x, t has negative local kinetic energy is (cf (3.8))

$$P_{\mathrm{neg}} = \frac{1-r_{\mathrm{neg}}}{2}, \tag{5.15}$$

where now (cf (3.9))

$$r_{\mathrm{neg}} \equiv \frac{\langle k_n^2\rangle}{\sqrt{\langle k_n^4\rangle}}. \tag{5.16}$$

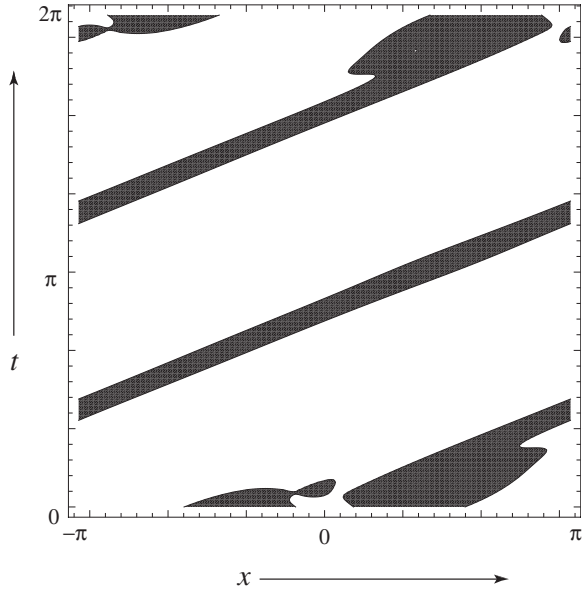

Figure 8. Negative kinetic energy regions in spacetime (black), for the initial wave (4.1) with $a = 0.5$ and $N = 6$.

From the fact that all k_n are non-zero, it follows that $P_{\text{neg}} \geqslant P_{\text{back}}$; the proof uses symmetrization of the sums for $r^2_{\text{back}} - r^2_{\text{neg}}$ and the relation

$$a^3 + b^3 + c^3 - 3abc = \tfrac{1}{2}(a+b+c)((a-b)^2 + (a-c)^2 + (b-c)^2) \geqslant 0 \tag{5.17}$$

for positive semidefinite a, b, c.

For the nonrandom initial state (4.1), $\Psi(x, t)$ exhibits strong negative energy for short times, but evolution soon randomises the phases, and as with backflow the negative-energy regions soon shrink to a fraction determined by P_{back}. For this function, with its concentrated fourier spectrum (4.5), (5.15) and (5.16) give, for large N,

$$P_{\text{neg}} \approx \frac{1}{2Na} \tag{5.18}$$

– four times larger than its backflow counterpart (4.7), as figure 8 illustrates, when compared with figure 5.

6. Optical retro-propagation

The wave $\psi(x)$ in (1.1) can also be regarded as the boundary value $\Psi(x, 0)$ of a monochromatic scalar wave $\Psi(x, z)$ with wavenumber K (representing a light beam, for example), travelling in the positive z direction in the x, z half-plane. Solution of the Helmholtz equation then gives the representation

$$\Psi(x, z) = \sum_{n=0}^{N} c_n \exp\left\{\mathrm{i}\left(k_n x + z\sqrt{K^2 - k_n^2}\right)\right\}. \tag{6.1}$$

Here we are concerned only with nonevanescent waves, for which $|k_n| < K$ for all n.

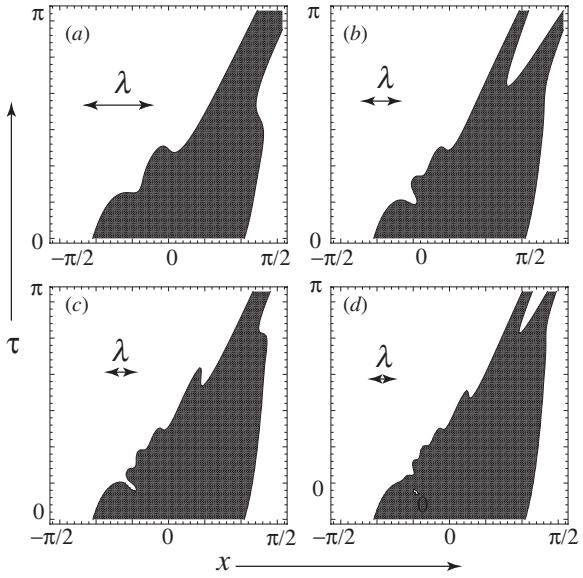

Figure 9. As figure 6, for the exact propagating beam (6.1) with $K = \frac{2}{\sqrt{3}}N$ and $z = \frac{2}{\sqrt{3}}\tau$, with wavelengths $\lambda = 2\pi/K$ indicated.

If all the k_n are positive semidefinite, the situation is similar to that studied in earlier sections: backflow corresponds to local propagation leftwards (towards negative x), even though every constituent plane wave is travelling to the right. And if $\max(k_n) \ll K$ it is possible to replace (6.1) by its paraxial approximation, which is identical with the Schrödinger equation (5.1), with z replacing t after suitable scaling. Backflow in the x, z plane is then identical with that already demonstrated in the spacetime plane x, t, including, for boundary functions $\psi(x)$ that are periodic, the optical analogue of quantum revivals, namely the Talbot effect [15, 16]): periodicity of the wave pattern in z as well as x.

Numerics confirms that the shape of the backflowing regions is not sensitive to the paraxial approximation. This is illustrated in figure 9, which corresponds to a beam in the form of an oblique fan of plane waves making directions with the z axis between 0° and 60°, that is $K = \gamma k_{\max} = \gamma N$, where $\gamma = \frac{2}{\sqrt{3}}$. To facilitate comparison with figure 6, figure 9 plotted in terms of the variable τ in (5.2) and (5.5), identified with z by expansion of the square roots in (6.1) as $\tau = z/\gamma$. Even for this scarcely paraxial 60° beam the shape of the region of strong backflow is similar to that in the paraxial approximation (figure 6). An unexpected consequence is that the strong backflow persists after propagation through many wavelengths $\lambda = 2\pi/K$: backflow survives until $\tau \sim \pi$, which corresponds to $z/\lambda = zK/2\pi \sim \gamma^2 N/2 \gg 1$.

More interesting than transverse backflow is the z dependence, embodied in the z component $k_z(x, z)$ (equation (1.5)) of the local wavevector. This can be negative ('retro-propagation'), even though the z components

$$k_{z,n} = \sqrt{K^2 - k_n^2} \tag{6.2}$$

of all constituent waves are positive. Now it is no longer necessary to assume that all the k_n are positive semidefinite. Retro-propagation is illustrated in figure 10 for the 21-wave beam

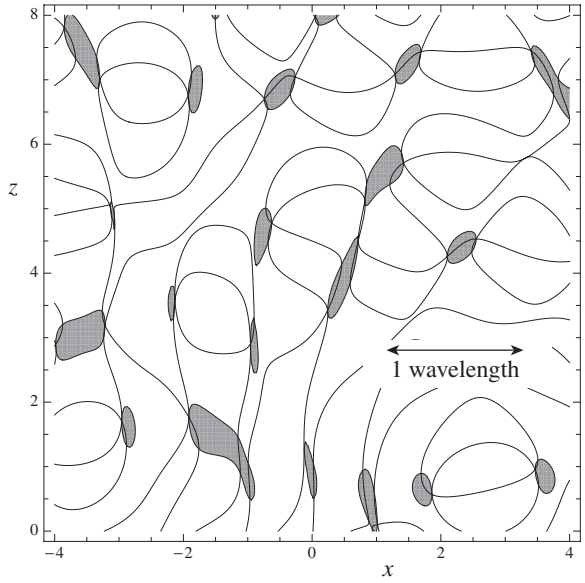

Figure 10. Regions of retro-propagation (gray), superimposed on phase contours at intervals of $\pi/2$, for the 21-wave beam (6.3).

$$N = 20, \qquad K = \pi, \qquad k_n = \pi \sin\left(\frac{\pi}{20}(n-10)\right), \\ c_n = \exp(\mathrm{i}\phi_n), \qquad \phi_n = \text{random on } [0, 2\pi]. \tag{6.3}$$

Superimposed on the figure are the wavefronts: contours of $\Psi(x, z)$, illustrating the fact (section 1) that the boundaries of the retro-propagating regions include the phase singularities (intersections of phase contours) and are tangent to the z direction at these points. In figure 10, approximately half of the retro-propagating regions include one phase singularity, and half include two; calculating correponding fractions in the general case seems a difficult statistical problem. Note that the regions of backflow are considerably smaller than the wavelength; this reflects the well-known fact that in the neighbourhood of phase singularities wavefunctions can vary on sub-wavelength scales.

It is evident that the retro-propagating regions are small. To understand why, we observe that for typical superpositions with $N \gg 1$ their measure (probability) is, from preceding theory

$$P_{\text{retro}} = \frac{1 - r_{\text{retro}}}{2}, \tag{6.4}$$

where (cf (3.9) and (5.16))

$$r_{\text{retro}} \equiv \frac{\langle k_{z,n} \rangle}{\sqrt{\langle k_{z,n}^2 \rangle}}. \tag{6.5}$$

To illustrate this, we note that the x wavenumber k_n corresponds to waves travelling at an angle $\theta_n = \sin^{-1}(k_n/K)$ to the z axis, and consider a superposition of many plane waves uniformly distributed between $\pm\theta_{\max}$; paraxiality corresponds to $\theta_{\max} \ll \pi/2$, and figure 10 represents

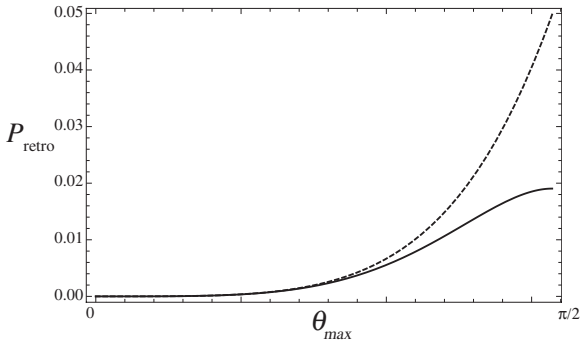

Figure 11. P_{retro} (equations (6.4) and (6.5)) as a function of beam angular half-width $\theta_{\max}$, for a uniform distribution of transverse wavevector components (full curve, from equation (6.6)) and propagation angles (dashed curve, from equation (6.7)).

the opposite case of $\theta_{\max} = \pi/2$. If this is interpreted as uniformity in k_n, that is, in $\sin\theta$, (6.4) gives

$$r_{\text{retro}} = \frac{\left(\frac{\theta_{\max}}{\sin\theta_{\max}} + \cos\theta_{\max}\right)}{2\sqrt{1 - \frac{1}{3}\sin^2\theta_{\max}}}, \tag{6.6}$$

while for uniformity in θ

$$r_{\text{retro}} = \frac{\sqrt{2}\sin\theta_{\max}}{\theta_{\max}\sqrt{1 + \frac{\sin 2\theta_{\max}}{2\theta_{\max}}}}. \tag{6.7}$$

As figure 11 shows, both distributions lead to very small values of P_{retro}. The largest value is 0.050, corresponding to a superposition of plane waves uniformly distributed in θ over the full range $\pm\pi/2$; in figure 10, corresponding to this case, the measured value of P_{retro} is 0.057, in reasonable agreement with the theoretical value. For paraxial beams, (6.5) and (6.6) both give

$$P_{\text{retro}} \approx \frac{\theta_{\max}^4}{180} \quad \left(\theta_{\max} \ll \tfrac{1}{2}\pi\right) \tag{6.8}$$

Even for a 45° beam ($\theta_{\max} = \pi/4$), P_{retro} is very small: close to 0.002 for both distributions (6.6) and (6.7).

Acknowledgments

I am grateful to Professor Gonzalo Muga for introducing me to backflow and for his hospitality in Bilbao where this work was begun, and to Professor Sandu Popescu for suggesting the study of time evolution. My research is supported by the Leverhulme Trust.

References

[1] Allcock G R 1969 The time of arrival in quantum mechanics III. The measurement ensemble *Ann. Phys.* **53** 311–48

[2] Bracken S J and Melloy G F 1994 Probability backflow and a new dimensionless quantum number *J. Phys. A: Math. Gen.* **27** 2197–211

[3] Muga J G, Palao J P and Leavens C R 1999 Arrival time distributions and perfect absorption in classical and quantum mechanics *Phys. Lett.* A **253** 21–7
[4] Muga J G and Leavens C R 2000 Arrival time in quantum mechanics *Phys. Rep.* **338** 353–438
[5] Dennis M R, Hamilton A C and Courtial J 2008 Superoscillation in speckle patterns *Opt. Lett.* **33** 2976–8
[6] Berry M V and Dennis M R 2009 Natural superoscillations in monochromatic waves in D dimensions *J. Phys. A: Math. Theor.* **42** 022003
[7] Born M and Wolf E 2005 *Principles of Optics* (London: Pergamon)
[8] Berry M V 1994 *Faster than Fourier in Quantum Coherence and Reality; in Celebration of the 60th Birthday of Yakir Aharonov* ed J S Anandan and J L Safko (Singapore: World Scientific) pp 55–65
[9] Kempf A and Ferreira P J S G 2004 Unusual properties of superoscillating particles *J. Phys. A: Math. Gen.* **37** 12067–76
[10] Berry M V and Popescu S 2006 Evolution of quantum superoscillations, and optical superresolution without evanescent waves *J. Phys. A: Math. Gen.* **39** 6965–77
[11] Aharonov Y and Rohrlich D 2005 *Quantum Paradoxes: Quantum Theory for the Perplexed* (Weinheim: Wiley-VCH)
[12] Berry M V and Shukla P 2010 Typical weak and superweak values *J. Phys. A: Math. Theor.* **43** 354024
[13] DLMF 2010 *NIST Handbook of Mathematical Functions* (Cambridge: University Press) http://dlmf.nist.gov
[14] Muga J G, Seidel D and Hegerfeldt G C 2005 Quantum kinetic energies: an operational approach *J. Chem. Phys.* **122** 154106
[15] Patorski K 1989 The self-imaging phenomenon and its applications *Prog. Opt.* **27** 1–108
[16] Berry M V and Klein S 1996 Integer, fractional and fractal Talbot effects *J. Mod. Opt.* **43** 2139–64